



An efficient heart sound segmentation approach using kurtosis and zero frequency filter features

Sumitra Shukla ^{a,*}, Sachin Kumar Singh ^b, Debjani Mitra ^a

^a Department of Electronics Engineering, Indian Institute of Technology (ISM) Dhanbad, Dhanbad, Jharkhand, 826004, India

^b Department of Mechanical Engineering, Indian Institute of Technology (ISM) Dhanbad, Dhanbad, Jharkhand, 826004, India



ARTICLE INFO

Article history:

Received 24 March 2019

Received in revised form 30 October 2019

Accepted 8 November 2019

Available online 4 December 2019

Keywords:

Heart sound segmentation

Kurtosis

Zero frequency resonator

Hilbert envelope

Squared envelope

ABSTRACT

This paper proposes an efficient heart sound segmentation method for automatic detection of heart sounds. In this method, the abrupt change at the heart sound locations is considered as a cue factor for segmentation. The phonocardiogram signal is analysed by passing kurtosis of the signal envelope through zero frequency filter (ZFF). The impulses at the locations of S1 and S2 in the filtered signal are used for the localization of heart sound. The performance of proposed method is evaluated on a real clinical dataset PhysioNet/CinC Challenge Heart Sound (PhysioNet/CinC). A set of 120 heart sound recordings, consisting of normal heart sound as well as pathological heart sound, is considered for evaluation. The experimental result shows that the proposed algorithm achieves an average sensitivity of 98.61%, average positive prediction of 99.11% and average overall accuracy of 98.07%. The robustness of the proposed algorithm is verified using additive white Gaussian noise and respiratory noise.

© 2019 Elsevier Ltd. All rights reserved.

1. Introduction

Cardiovascular diseases (CVDs) are the most leading cause of mortality worldwide [1]. CVDs include arrhythmias, valve disease, and heart failure. Condition of heart can be ascertained by analysing the electrocardiogram (ECG) and phonocardiogram (PCG) signals. Though the ECG signal can reveal various abnormal behaviour of the heart, some of the symptoms such as heart murmurs, caused by defective heart valves, are difficult to be observed in the ECG signal [2]. Another approach to ascertain the heart condition is heart auscultation. The heart auscultation is the process to auscultate the sound produced by the mechanical activity of the heart valves and associated vessels [3,4]. An analysis of heart sound can give some valuable insights for the diagnosis of CVDs. However, an effective diagnosis of heart sound is limited by the physician's perception and the quality of hearing instruments [5]. PCG records the heart sounds. Therefore, the PCG signal can be used for visual depiction of heart sound. Also, the recorded PCG signal gives a scope for analysis of the heart sound signal. Signal processing analysis of the PCG signal helps in quantitative and qualitative characterization of the heart abnormalities. Hence, the signal processing analysis of

PCG signal is expected to improve the overall efficiency of the CVD classification.

Accurate segmentation of heart sound is required for effective automatic classification of the pathologic conditions of heart [2–6]. The fundamental heart sound (FHS) contains four parts: the 1st heart sound (S1), the 2nd heart sound (S2), the systolic period and the diastolic period. Any segmentation process first localizes the S1 and S2, and then the systolic and diastolic periods are decided based on the localised S1 and S2. The systolic interval is the interval from S1 to S2 and the diastolic interval is the interval from S2 to S1. The PCG signal also contains murmurs. These murmurs in systolic and diastolic intervals are associated with the dysfunctioning of the valves. Aortic stenosis (AS), mitral regurgitation (MR), mitral valve prolapse (MVP) and coronary artery disease (CAD) are the most frequent causes for the murmurs.

The segmentation of FHSs should give accurate positions of the heart sounds, S1 and S2, for better localization of the systolic and diastolic regions. Time-frequency based methods are used extensively to segment the heart sounds [7–11]. These methods mainly use the wavelet based decomposition techniques to provide the detailed time-frequency content of the PCG signal [9]. At a certain level of decomposition, the wavelet transform gives emphasis to the heart sounds while suppressing the murmurs and noises [9]. Daubechies [9], and Morlet [7] are used for wavelet based heart sound segmentation [10]. Kamson et al. [12] proposed logistic function amplitude moderator and Teager-Kaiser energy operator based

* Corresponding author.

E-mail addresses: sumitershukla1@gmail.com (S. Shukla), sachinsingh47@gmail.com (S.K. Singh), dejanimitra68@gmail.com (D. Mitra).

features for heart sound segmentation. Courtemanche et al. [13] proposed heart sound segmentation algorithm using Mel-scaled wavelet transform by modifying Mel frequency cepstral coefficient algorithm using discrete wavelet transform in order to reduce the effect of the noise from the cepstral coefficients. These coefficients were further used for segmentation of the heart sounds. Zhang et.al [14] proposed matching pursuit based decomposition technique for heart sound segmentation. Hilbert-Huang transform (HHT) is also a popular decomposition technique used for heart sound segmentation [5,15]. HHT decomposes a signal into a finite number of nearly mono-component signals, called the intrinsic mode functions (IMFs) [5]. Papadaniil and Hadjileontiadis [5] analysed heart sound signal by decomposing it into IMFs. The kurtosis of these IMFs was used to detect abrupt changes that occur at the locations of S1 and S2. The main limitation of this technique is the selection of IMFs for heart sound segmentation under varying temporal-spectral characteristics of heart sound, murmurs, and background noises.

Envelop based segmentation methods identify the cardiac cycle by analysing envelop of the PCG signal. In these methods, envelop of the heart sound signal is extracted using various approaches such as Shannon energy envelop [16,17], Shannon entropy envelop [2] and Hilbert envelop [18]. Sepehri et al. [19] extracted envelop of the heart sound signal by using short-time spectral energy and autoregressive parameters of the signal. Yan et al. [18] used Viola integral method to calculate multi-scale characteristic waveform of heart sound and its characteristic moment waveform. The multiscale moment analysis was used to locate each cycle of heart sound. In general, the envelop extraction algorithm is performed either in time domain [17], or in Hilbert transform domain [18], or in wavelet transform domain [9]. Normally, the energy envelop criterion requires amplitude-dependent threshold for segmentation of the heart sounds. In this criterion, only those peaks are considered to belong the heart sounds that have higher energies than a threshold. Sometimes this criterion eliminates some genuine heart sounds with less energy. In order to overcome this problem, duration information between heart sounds is incorporated in the segmentation algorithm. Fanfulla et al. [20] incorporated fuzzy logic for heart sound segmentation for arrhythmias patients. Tang et al. [21] introduced density function based dynamic clustering after decomposing the PCG signal into a number of atoms characterized by timing delay, frequency, amplitude, time width, and phase. Gill et al. [22] proposed a probabilistic approach to detect heart sound by using hidden Markov model (HMM). Springer et al. [23] developed a heart sound segmentation algorithm using logistic regression hidden semi Markov model (LHSMM). Kamson et al. [24] proposed multi-centroid diastolic duration model for HSMM based heart sound segmentation. In this method, the centroids were calculated by hierarchical agglomerative clustering using Ward's method. The majority of existing methods focuses on envelope based feature to detect peak at the heart sound location. The signal envelope mainly captures the sound intensity. However, the envelope of the signal is often distorted by noise. As a result, a threshold based technique or a duration modelling technique may not be effective in detecting the heart sounds, specially, when the strength of heart sounds is weak due to pathological conditions.

The important cue factors for segmentation of the heart sounds are (i) occurrence of heart sounds S1 and S2, and (ii) durations between S1 to S2 and that between S2 to S1. The occurrence of heart sounds, S1 and S2, produces abrupt changes in the signal. The objective of this paper is to emphasise the importance of abruptness induced due to occurrence of heart sounds. In the present work, a new technique is proposed to localize the heart sounds S1 and S2 by detecting these abrupt changes. This technique is based upon passing kurtosis of the signal envelope to the ZFF for detecting the impulsiveness. The kurtosis of the signal envelope increases the

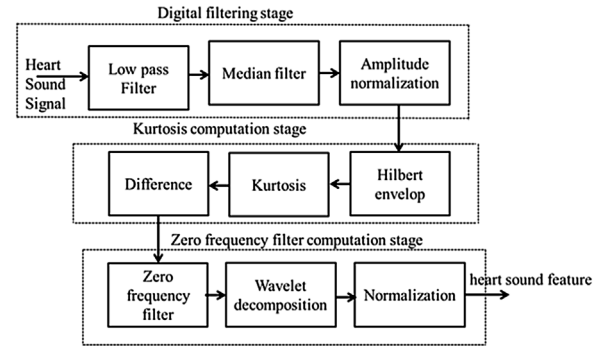


Fig. 1. Block diagram of proposed heart sound feature extraction.

strength of the abrupt changes at the heart sound locations. Then, the ZFF preserves the information of abrupt changes in a signal. The organisation of the paper is as follows. The description of proposed methodology for heart sound segmentation is given in Section 2. The evaluation of proposed method using heart sound database is described in Section 3. Finally, conclusion of the present study is discussed in Section 4.

2. The proposed methodology for heart sound segmentation

The correct estimation of the occurrence of heart sounds is the most important factor for the localization of heart sounds. The occurrence of heart sound produces abrupt changes in the signal [5]. These abrupt changes can be used to locate the heart sounds S1 and S2. However, it is difficult to observe these abrupt changes due to pathological conditions and environmental noises. In the present work, a three step approach is used to extract the impulses at the heart sound locations in the PCG signal. The first step obtains the envelope of the signal. The Hilbert envelope gives peaks at approximate locations of the heart sounds [25]. The second step computes the kurtosis of the signal envelope to get impulse-like characteristics at the heart sound locations. In the third step of this algorithm, the kurtosis of the signal is passed through ZFF to keep only the impulse information in the signal. These extracted impulse information is considered to be feature for the heart sound segmentation. The proposed feature extraction technique for heart sound segmentation is shown in Fig. 1.

The proposed feature extraction technique includes three stages. The first stage is digital filtering stage which includes a low-pass filter, a median filter, and an amplitude normalization to emphasize the heart sounds signal and to remove the noises from the signal. In the second stage, kurtosis of the Hilbert envelop of signal is estimated to increase the impulsiveness of the signal. The third stage includes zero frequency filtering operation to preserve only the impulse information in the signal. Wavelet decomposition is used to extract these impulse information from the ZFF output. The decomposed signal is then normalized by subtracting from its mean and dividing by its standard deviation in order to avoid variability due to inter-patients heart sounds.

2.1. Enhancement of heart sound and noise suppression

In real environment, the heart sound signal may be corrupted by various kinds of ambient noises and physiological sounds, such as intestinal and breathing sounds. Therefore, a low pass filter is constructed to reduce the effect of noise [5]. The signal is filtered with a 20th order linear phase low-pass FIR filter with a cut-off frequency of 100 Hz. The sampling frequency of the input signal is 1000 Hz. Then, the filtered signal is passed through a 10th order median filter

to enhance the quality of the acquired signal. For the filtered heart sound signal, $x_1[n]$, zero mean and amplitude normalisation of the signal are done as per Eq. (1) and Eq. (2), respectively.

$$x'[n] = x_1[n] - \frac{1}{N} \sum_{n=1}^N x_1[n] \quad (1)$$

$$x[n] = \frac{x'[n]}{\sum_{n=1}^N (|x'[n]|)} \quad (2)$$

Here, $x[n]$ is the zero mean and amplitude normalized signal. N is the length of the heart sound signal, $x_1[n]$.

2.2. Kurtosis computation of the Hilbert envelope of the signal

Kurtosis of a signal is the ratio of fourth central moment and squared second central moment of the signal [26]. Kurtosis is considered as a measure for the impulsiveness of a signal. The occurrence of heart sound produces abrupt changes in the PCG signal [5]. As a result, transient impulses corresponding to heart sounds occur cyclically in the PCG signal. These transient impulses lead to instantaneous energy fluctuations in the PCG signal at the heart sound locations. Hence, kurtosis of the signal contains peaks at these fluctuations. Impulsiveness of the signal at these locations can be improved by taking envelop of the signal. This is due to unipolar nature of the envelop signal [25]. As a result, kurtosis of the signal envelope gives localized peaks at the heart sound locations.

Envelop of a signal is obtained from the analytic function. The analytic function, $\tilde{x}_h[n]$, of the filtered signal is given by [25],

$$\tilde{x}_h[n] = x[n] + jx_h[n] \quad (3)$$

Here, $x_h[n]$, is the Hilbert transform of the PCG signal. The envelope of the signal is,

$$|\tilde{x}_h[n]| = |x[n] + jx_h[n]| \quad (4)$$

The squared envelop, $SE[|\tilde{x}_h[n]|]$, is calculated as absolute squared value of the analytical signal,

$$SE[|\tilde{x}_h[n]|] = |\tilde{x}_h[n]|^2 \quad (5)$$

The kurtosis, $k[|\tilde{x}_h[n]|]$, of the zero-mean signal envelope, $|\tilde{x}_h[n]|$, is given by,

$$k[|\tilde{x}_h[n]|] = \frac{E(|\tilde{x}_h[n]|^4)}{[E(|\tilde{x}_h[n]|^2)]^2} \quad (6)$$

where, $E(\cdot)$ stands for the expectation operation. In order to capture transient impulse around the heart sound location, a short time kurtosis of the signal is computed by taking a rectangular window. The length of the window is an important parameter for capturing the transient impulse information. In FHS, the diastolic interval length is higher than the systolic interval length [27]. In this study, the size of window is chosen to be less than the systolic interval so as to capture transient impulse information from a single heart sound (either S1 or S2) in a particular window. For larger window size, the transient information may get affected by the presence of other heart sounds present in that window. In general, the normal range of systolic time interval is more than 0.3 sec. Therefore, the length of window is chosen to be 0.2 sec with an overlap of 1 msec. The short time kurtosis of the signal envelope, for a given window w , is given as,

$$k[|\tilde{x}_h^w[n]|] = \frac{E(|\tilde{x}_h^w[n]|^4)}{[E(|\tilde{x}_h^w[n]|^2)]^2} \quad (7)$$

The heart sound signal after pre-processing is expected to be zero mean signal, therefore, fourth moment of the signal envelope can be estimated as,

$$E(|\tilde{x}_h^w[n]|^4) = \frac{1}{N_w} \sum_{n=t}^{t+N_w-1} |\tilde{x}_h[n] w[n-t]|^4 \quad (8)$$

where, N_w is the length of the sliding window $w[n]$. In this paper, the kurtosis vector is calculated by giving one sample shift.

Fig. 2 shows the kurtosis of the signal envelope of a PCG signal taken from real clinical environment. **Fig. 2(d)** and **Fig. 2(e)** show kurtosis of signal and kurtosis of signal envelope of the PCG signal, respectively. It is observed from the figure that the kurtosis of the signal envelope has stronger peaks at heart sound locations compared to kurtosis of the signal without considering envelope. From **Fig. 2(b)** and **2(c)**, it can be observed that the squared envelope of the signal has more clear impulses at the heart sound locations compared to the signal envelope. This has a role in improving the kurtosis of the signal in **Fig. 2(e)**. In order to understand the role of squared envelope in kurtosis computation, this study describes a relation between kurtosis of signal envelope and squared envelope of the signal.

The kurtosis of signal envelope, given in Eq. [7], can be written as,

$$E(|\tilde{x}_h^w[n]|^4) = \frac{1}{N_w} \sum_{n=t}^{t+N_w-1} (SE[\tilde{x}_h^w[n]])^2 \quad (9)$$

Right hand side of Eq.8 is equivalent to the squared-envelope (SE) of the windowed signal. Therefore,

$$E(|\tilde{x}_h^w[n]|^4) = \frac{1}{N_w} \sum_{n=t}^{t+N_w-1} (SE[\tilde{x}_h^w[n]])^2 \quad (10)$$

or,

$$E(|\tilde{x}_h^w[n]|^4) = E[SE[\tilde{x}_h^w[n]]]^2 \quad (11)$$

Similarly, the squared second central moment of signal envelope is,

$$\{E(|\tilde{x}_h^w[n]|^2)\}^2 = \{E[SE[\tilde{x}_h^w[n]]]\}^2 \quad (12)$$

The kurtosis of signal envelope can now be written as,

$$k[|\tilde{x}_h^w[n]|] = \frac{E[SE[\tilde{x}_h^w[n]]]^2}{\{E[SE[\tilde{x}_h^w[n]]]\}^2} \quad (13)$$

The normalized variance of $SE[\tilde{x}_h^w[n]]$ is defined as the ratio between variance of $SE[\tilde{x}_h^w[n]]$ and the square of the expectation of $SE[\tilde{x}_h^w[n]]$. The normalized variance of $SE[\tilde{x}_h^w[n]]$ can be written as,

$$d[SE[\tilde{x}_h^w[n]]] = \frac{var[SE[\tilde{x}_h^w[n]]]}{\{E[SE[\tilde{x}_h^w[n]]]\}^2} \quad (14)$$

The variance of $SE[\tilde{x}_h^w[n]]$ can be expressed as expectation of the square of $SE[\tilde{x}_h^w[n]]$ minus the square of the expectation of $SE[\tilde{x}_h^w[n]]$ [28],

$$var[SE[\tilde{x}_h^w[n]]] = E[SE[\tilde{x}_h^w[n]]^2] - \{E[SE[\tilde{x}_h^w[n]]]\}^2 \quad (15)$$

Substituting for $var[SE[\tilde{x}_h^w[n]]]$ from Eq. (14)

$$d[SE[\tilde{x}_h^w[n]]] = \frac{E[SE[\tilde{x}_h^w[n]]]^2}{\{E[SE[\tilde{x}_h^w[n]]]\}^2} - 1 \quad (16)$$

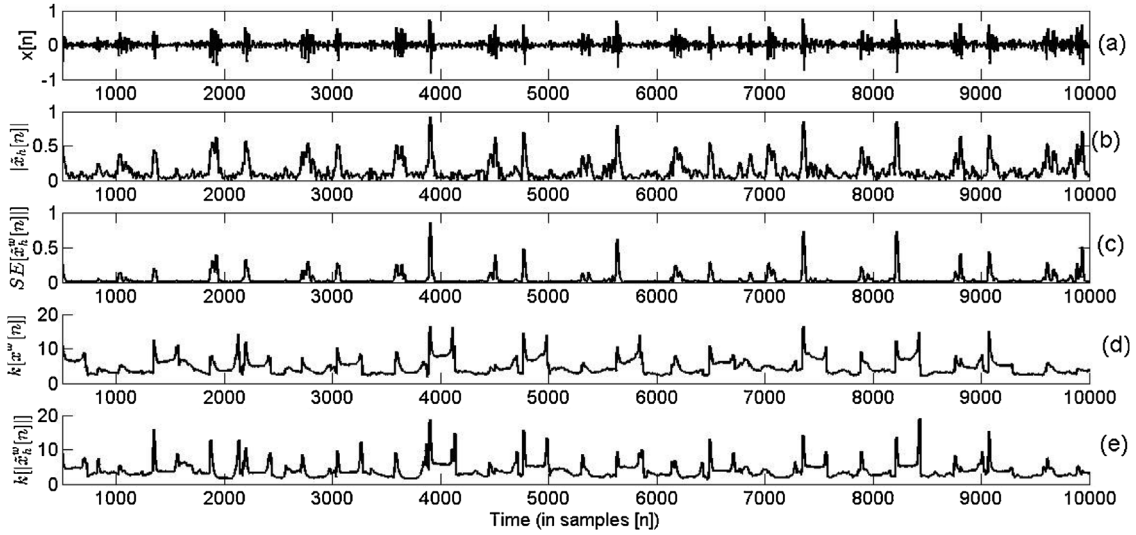


Fig. 2. Kurtosis of the signal envelope, (a) PCG signal, (b) envelope of the signal, (c) squared envelope of the signal, (d) kurtosis of the signal without considering envelope of the signal and (e) kurtosis of the signal after considering envelope of the signal.

substituting Eq. 16 in Eq.13,

$$k \left[|\tilde{x}_h^w[n]| \right] = d \left[SE \left[\tilde{x}_h^w[n] \right] \right] + 1 \quad (17)$$

From Eq. (17), it can be inferred that the kurtosis of the signal envelope is equivalent to the normalized variance of the squared envelope of the signal. The role of squared envelope in increasing the variance at the impulse locations is explained in Fig. 2.

Fig. 2(b) and Fig. 2(c) show signal envelope and squared envelope of the PCG signal, respectively. It can be observed that the squared envelope of the signal reduces the effect of the high frequency fluctuation and dominant peaks are observed at the heart sound locations. As a result, the variance of the squared envelope of signal is more compared to the variance of the signal without envelope. The increase in the variance of the signal envelope increases the kurtosis values at the heart sound location. Therefore, kurtosis of the signal envelope has strong peaks at heart sound locations compared to kurtosis of the signal without considering envelope. The same observation is observed for the PCG signal contaminated with physiological noise, shown in Fig. 3. The kurtosis of the signal envelope has strong peaks compared to kurtosis of signal without envelop. It can be inferred that the kurtosis of the signal envelope gives more prominent impulses at the heart sound locations compared to the kurtosis of the signal without considering envelope.

2.3. Zero frequency filter

The transient impulses corresponding to heart sounds produce instantaneous energy fluctuation in the PCG signal and it gives peaks in kurtosis of the signal envelope. Difference of the kurtosis along time axis is taken in order to increase the impulsiveness of kurtosis of the signal envelope. Here, difference of the kurtosis of the signal envelope is referred as kurtosis signal. Fig. 4 illustrates the kurtosis signal of a PCG signal added with simulated white noises at different SNR values of 30 dB, 20 dB and 10 dB. Figure shows that the kurtosis signal removes small fluctuations at locations where heart sound is not present and increases the strength of the impulses around the heart sound locations. In some cases, however, the strength of heart sound S2 is very low. When the signal is contaminated by noise, these weak sounds get overridden by the noises. Therefore, the kurtosis of the signal envelope contains weak impulses at these locations of the heart sounds as shown in Fig. 4 by circles. Though, these impulses are weak to be observed, the information of these impulses are still present in the kurtosis sig-

nal. Hence, in the present work, impulse like characteristics around S1 and S2 is extracted by passing the kurtosis signal through ZFF [29,30]. ZFF is basically a resonator of second order infinite impulse response (IIR) filter with a complex conjugate pair of poles located on unit circle [29]. The centre frequency of the resonator is chosen at zero Hz. The energy of an impulse lies uniformly at all frequencies. The output of the filter thus contains DC value along with fluctuations at impulse locations. The difference equation corresponding to zero frequency filter is given by

$$y[n] = - \sum_{k=1}^2 a_k y[n-k] + k' \left[\tilde{x}_h^w[n] \right] \quad (18)$$

and the corresponding transfer function is given by

$$H[z] = \frac{Y[z]}{K' \left[\tilde{x}_h^w[z] \right]} = \frac{1}{1 + a_1 z^{-1} + a_2 z^{-2}} \quad (19)$$

where, $a_1 = -2$ and, $a_2 = 1$. $Y[z]$ and $K' \left[\tilde{x}_h^w[z] \right]$ are the z-transforms of filter output $y[n]$ and filter input i.e. kurtosis signal, $k' \left[\tilde{x}_h^w[n] \right]$, respectively. The pole of this transfer function lies on $z = 1$. The output of ZFF is basically equivalent to two times successive integration of the input signal. The resonator output grows/decays approximately as a polynomial function of time.

The output of the ZFF gets fluctuation at the impulse locations in the input kurtosis signal. However, these fluctuations in the output signal are small in amplitude and are hidden in large amplitude value of the filtered output. Therefore, it is difficult to extract the location of the impulses. In this study, the fluctuation due to impulse is obtained by decomposing the filtered signal using discrete wavelet transform. At particular decomposition level, the detailed coefficient contains only impulse information. The wavelet family and decomposition levels were determined experimentally. The wavelet reverse biorthogonal 3.9 is found to be suitable with third level of decomposition [23]. The absolute value of the detail coefficients is computed in order to get impulses at the heart sound locations. Here, the absolute value of detailed coefficients is termed as residual signal.

Fig. 5 shows output of the ZFF of the PCG signal. The kurtosis signal, shown in Fig. 5(b), is passed through ZFF. The output of filter is shown in Fig. 5(c). Fluctuations at impulse locations are not observable due to its small amplitude compared to large DC value. The residual output of the signal after wavelet decomposi-

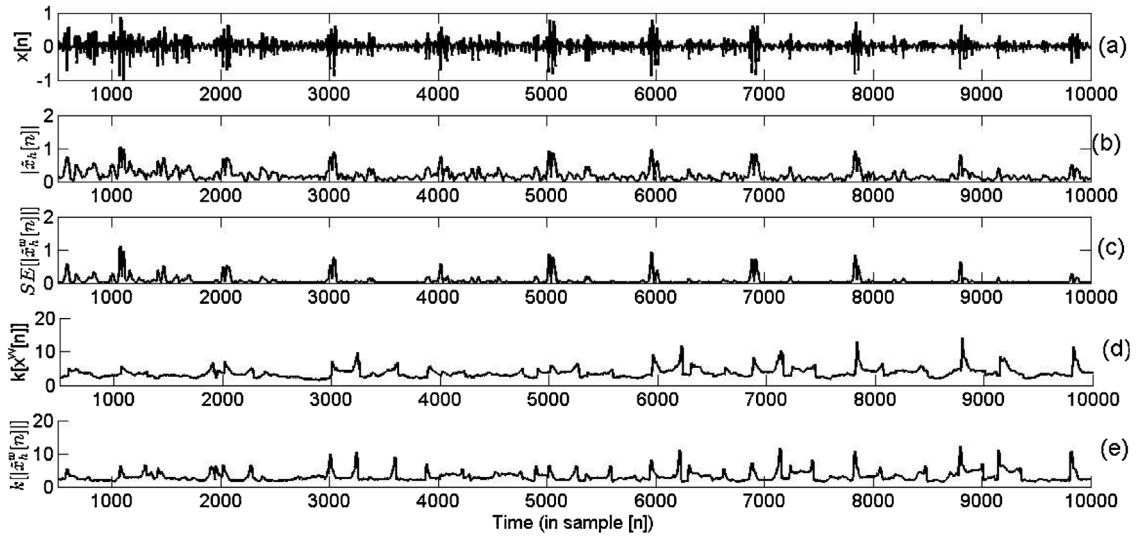


Fig. 3. Kurtosis of the signal envelope of the PCG signal contaminated with physiological noise, (a) PCG signal, (b) envelop of the signal, (c)squared envelop of the signal and (d) kurtosis of the signal without considering envelope of the signal and (d) kurtosis of the signal after considering envelope of the signal.

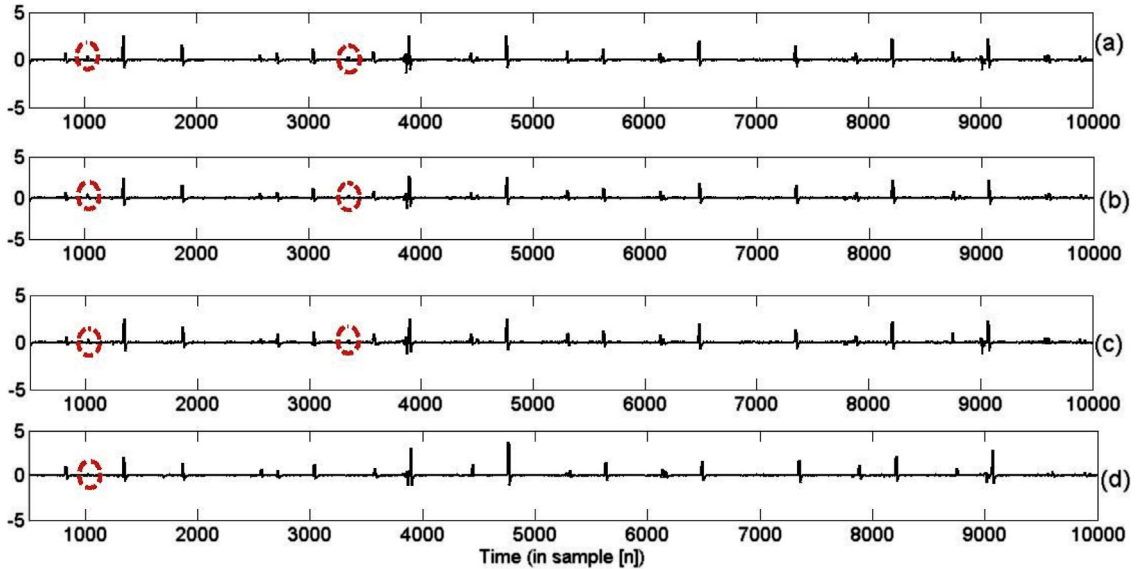


Fig. 4. Kurtosis signal. Here, y axis depicts kurtosis of PCG signal, (a) PCG signal, (b) PCG signal with 30 dB, (c) PCG signal with 20 dB, and (d) PCG signal with 10 dB.

tion is shown in Fig. 5(d). Figure shows that the residual output contains clear impulses at the heart sound locations only. Fig. 6 shows the residual outputs at different noise levels. Figure shows that residual output contains impulses at those locations where the impulses were difficult to be observed in the kurtosis signal, shown in Fig. 4 by circles. In Fig. 6, these impulses are highlighted by circles. Hence, the residual output retains not only the strong impulses; it also retains the weak impulses of the kurtosis signal. Hence, it is expected that zero frequency filtering will preserve the impulse information for PCG signal contaminated with different pathological conditions and environmental noises.

2.4. Duration modelling using HMM based method

The second most important cue point for segmentation of heart sound is to model duration between sound S1 and S2. In the present work, the duration modelling of heart sounds is done as described by Springer [23]. In this study, four state HMM is used to model

each of the four major components of the heart cycles. These are S1 duration, systolic period, S2 duration and diastolic period. During training phase, the PCG signal is taken from conditions: normal, murmurs relating to MVP and aortic disease. The block diagram of the heart sound segmentation is shown in Fig. 7.

During training phase, the extracted feature of the PCG signal along with the heart sound labels are given as inputs to train the model using hidden semi Markov model. The labels of S1 and S2 sounds in the PCG signal are estimated depending upon the locations of R-peaks and the end of T-waves in the ECG signal, respectively. In this study, explicit duration information is incorporated in the HMM [23,24]. Hidden semi Markov model is defined as, $\lambda = \{A, B, \pi, P\}$, where,

$A = \{a_{ij}\}$ is the transition probability from state i at time t to state j at time $t + 1$.

$B = \{b_j(o_t)\}$; $1 \leq j \leq N$ is the observation probability of state j that generates the observation sequence o_t at time t . N is the number of states.

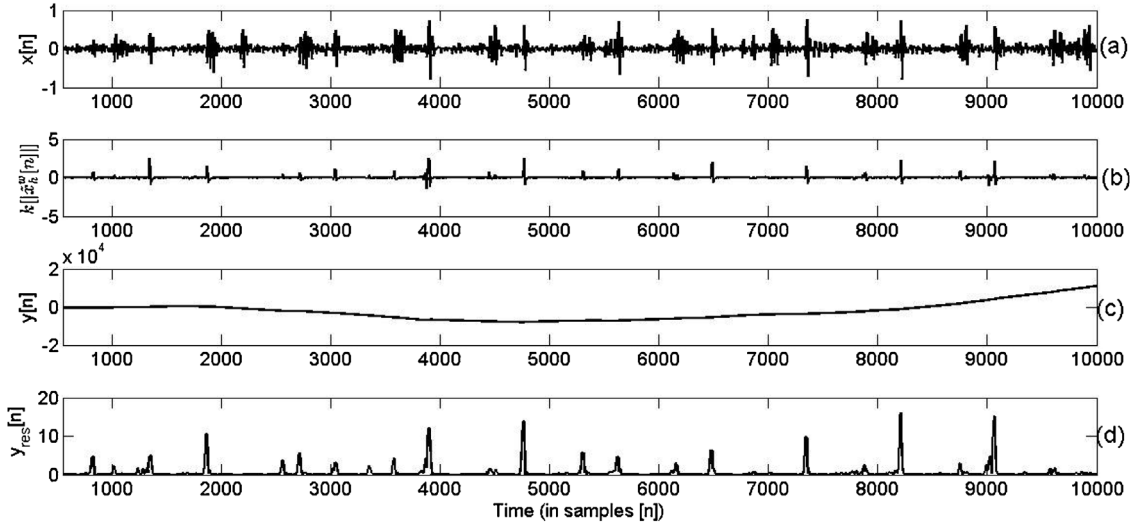


Fig. 5. Residual outputs of the ZFF (a) PCG signal, (b) kurtosis signal, (c) output of the ZFF, and (d) residual output of the signal.

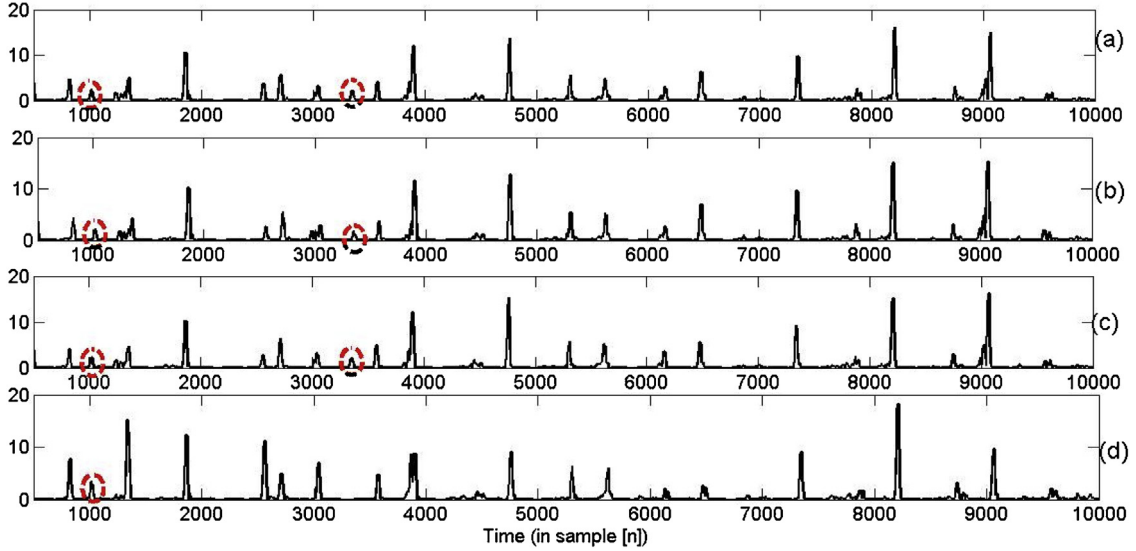


Fig. 6. Residual outputs. Here, y axis depicts residual output of PCG signal, (a) PCG signal, (b) PCG signal with 30 dB, (c) PCG signal with 20 dB, and (d) PCG signal with 10 dB.

$\pi = \{\pi_i\}$ is the initial state probability that defines of being in state i at the first time $t = t_1$.

$P = \{p_i(d)\}$ is the duration probability of being in state i for duration d .

For heart sound segmentation, the optimal state sequence for a given model, λ , and for a given observation sequence, o_t , is estimated by a dynamic programming method called Viterbi algorithm. In this study, Viterbi algorithm is modified by incorporating duration model for each state. Then, the state likelihood for state j at time t is defined as

$$\delta_t(j) = \max_d \left[\max_{i \neq j} [\delta_{t-d}(i) \cdot a_{ij}] \cdot P_j(d) \cdot \prod_{s=0}^{d-1} b_j(o_{t-s}) \right] \quad (20)$$

with $1 \leq i, j \leq N$, $1 \leq t \leq T$, and $1 \leq d \leq d_{max}$, where, d_{max} is the maximum expected time to remain in any one state.

The state likelihood is maximized by tracking two arguments, the corresponding duration and the past state, at each

instant of time, t , and storing the arguments in $D_t(j)$ and $\psi_t(j)$, respectively.

$$D_t(j) = \operatorname{argmax}_d \left[\max_{i \neq j} [\delta_{t-d}(i) \cdot a_{ij}] \cdot P_j(d) \cdot \prod_{s=0}^{d-1} b_j(o_{t-s}) \right] \quad (21)$$

$$\psi_t(j) = \operatorname{argmax}_{i \neq j} [\delta_{t-d}(i) \cdot a_{ij}], 1 \leq i \leq N \quad (22)$$

In Viterbi algorithm, the state sequence starts at the observation sequence starting instant. Similarly, the state sequence ends at the observation sequence ending instant. However, the PCG signal recording starts and stops at any stage of heart cycle. In order to resolve this problem, the most likelihood state sequence is obtained by using extended back tracking algorithm called extended Viterbi algorithm [23]. This algorithm extrapolates the state likelihood beyond the beginning and ending of the PCG sequence while considering observations from within the PCG sequence.

In this paper, approximately two hundred recordings from normal and pathological conditions are considered for training. A non-ergodic HMM is developed where S2 has to precede diastolic;

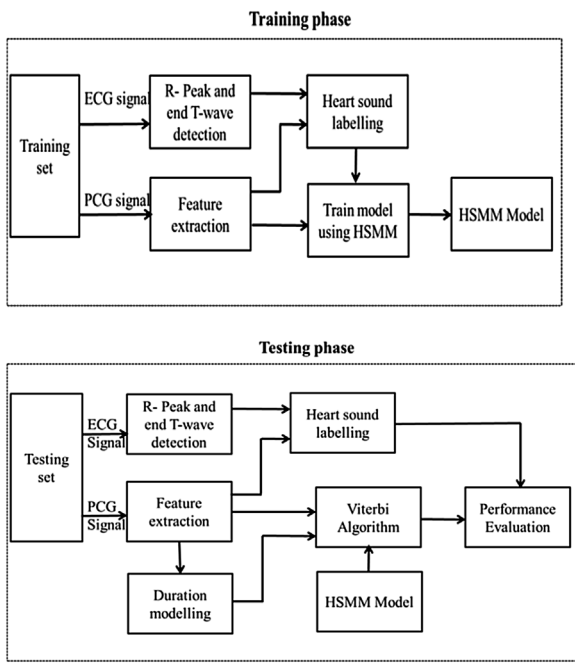


Fig. 7. Block diagram of HSMM based heart sound segmentation [23].

diastolic cannot be preceded by systolic or S1. Approximately, one hundred twenty PCG recordings from both normal and pathological conditions are considered for evaluation of proposed algorithm.

Fig. 8 shows segmentation of heart sound using proposed algorithm. **Fig. 8(b)** shows that the envelope of residual output gives peaks at the location of heart sounds. The duration between peaks corresponding to sound S1 and S2 is modelled using HMM. The Viterbi algorithm decides optimal state sequence corresponding to PCG signal. The state sequence contains S1 and S2 sound locations of PCG signal. These S1 and S2 locations are shown in **Fig. 8(c)** by dashed vertical lines. **Fig. 9** corresponds to the PCG signal taken from clinical noisy condition. From the **Fig. 9(b)**, it can be observed that the residual output contains clear peaks at the locations of the heart. The state sequence corresponding to noisy PCG signal is plotted in **Fig. 9(c)** by dashed vertical lines. Hence, the proposed algorithm is able to locate the heart sounds effectively in normal condition as well as in clinical noisy condition.

3. Result and Discussion

The proposed heart sound segmentation algorithm is evaluated using the PhysioNet/CinC Challenge Heart Sound (PhysioNet/CinC) [31,32] in order to evaluate the effectiveness of the proposed algorithm for localization of heart sound in pathological condition. The dataset consists of 792 PCG recordings with manually annotated R-peak and T-wave labels from ECG waveforms. The PCG signals are resampled at 1000 Hz and the ECG signals are sampled at 50 Hz. There are 135 patients and the heart sounds are recorded at various locations on the chest. The database is collected from the normal patients as well as from the patients with pathological conditions such as mitral valve prolapse (MVP). The reference positions for S1 and S2 sounds are decided by the R-peak and the end of T-wave positions that were computed from the synchronous ECG signals as described in [23]. The start of S1 sound coincides with the R-peaks of the ECG while the S2 sound occurs approximately at the end of T-wave in the ECG. S1 sound is considered to be identified correctly if the start of the segmented S1 is found to be within 100 ms of the R-peak in the ECG. Similarly, S2 sound is considered to be identified

correctly if the centre of S2 sounds is found to be within 100 ms of the corresponding end of T-peak.

The performance of the proposed algorithm can be evaluated on the basis of their sensitivity (Se) and the Positive Predictive Value (PPV), given in Eq.23 and Eq.24, respectively,

$$Se = \frac{TP}{TP + FN} \times 100\% \quad (23)$$

$$PPV = \frac{TP}{TP + FP} \times 100\% \quad (24)$$

Here, true positive (TP) refers to total number of correctly detected heart sounds in a given PCG signal. False negative (FN) refers to total number of heart sounds not correctly detected in a given PCG signal. False positive (FP) refers to total number of noisy segments detected as heart sounds [2]. The overall performance of the algorithm is measured in term of accuracy (Acc) and it is given in Eq.25 as,

$$Acc = \frac{TP}{TP + FP + FN} \times 100\% \quad (25)$$

Sensitivity, positive predictive value and overall accuracy all together decides the performance of an algorithm. Performance of the proposed algorithm is compared with state of the art method LHSMM [23] based heart sound segmentation method. The sensitivity, positive predictive value and accuracy of the algorithms are evaluated for each recording. Average sensitivity, average predictive value and average accuracy of the two algorithms are tabulated in **Table 1**. Performance of the algorithm is evaluated for 120 PCG recordings which contain a total of 3669 heart sounds. These recordings contain both normal and pathological heart sounds. The false negative and false positive of the proposed technique are 51 and 42, respectively whereas, the false negative and false positive of the LHSMM are 46 and 63, respectively. The proposed algorithm has higher false negative compared to LHSMM. On the other hand, the proposed technique has very less false positive. As a result, the positive predictive value of the proposed algorithm is higher than that of LHSMM with small reduction in sensitivity. Therefore, the overall accuracy of the proposed algorithm is 98.07% whereas the accuracy of LHSMM algorithm is 96.82%. The proposed algorithm predicts 99.11% correctly the location of the heart sounds, S1 and S2. Also, it is able to segment 98.61% correctly the heart sounds. Hence the present algorithm has good performance for both normal and pathological heart sounds.

The proposed algorithm is evaluated for different pathological heart sounds in order to compute the effectiveness of algorithm for pathological PCG signal. **Fig. 10** shows the segmentation of sounds S1 and S2 in the PCG signal taken from severe aortic stenosis condition. From **Fig. 10(b)**, it can be observed that the filtered output has peaks at the locations of heart sound. The effect of the murmur between S1 and S2 sounds is removed in the residual output. Hence, the algorithm gives accurate localization of heart sounds. Similar observation can be observed in case of PCG signal taken from MVP condition shown in **Fig. 11**. The residual output, shown in **Fig. 11(b)**, gives strong peaks at the locations of the heart sounds. The PCG signal contains impulsive clicks between S1 and S2, as shown in **Fig. 11(a)** by arrows. These clicks are for very short duration and they occurred close to S2 sound. The effect of these impulsive clicks is normalized with the sound S2 during kurtosis computation. Therefore, the peaks corresponding to these clicks are overlapped with the peaks of S2 sound as shown in **Fig. 11(b)**. In some cases, shown in **Fig. 11 (c)** by black circles, it is difficult to distinguish between the ending of clicks and the starting of sound S2. In such cases, the localization of sound S2 is difficult.

The proposed segmentation algorithm is evaluated for the PCG signal taken from arrhythmia condition, shown in **Fig. 12**. Here, the systolic interval and diastolic interval are nearly equal. In this case,

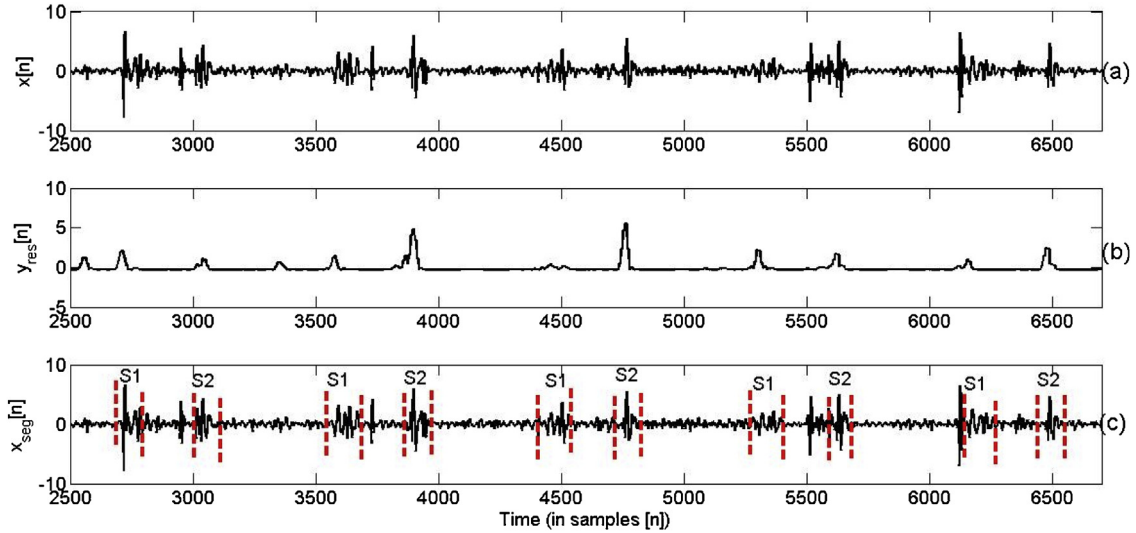


Fig. 8. Segmentation of heart sound using proposed algorithm where PCG signal is taken from clean environment. Dashed vertical lines show marking of heart sound using proposed algorithm (a) PCG signal, (b) residual output of ZFF, (c) segmentation marking of heart sounds.

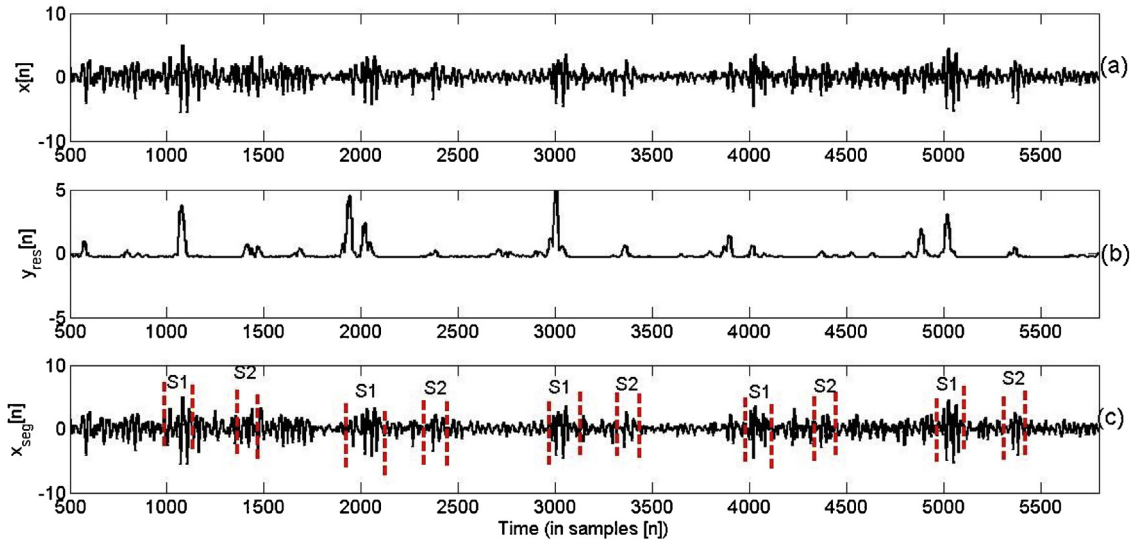


Fig. 9. Segmentation of heart sound using proposed algorithm where PCG signal is taken from clinical noisy condition. Dashed vertical lines show marking of heart sound using proposed algorithm (a) PCG signal, (b) residual output of ZFF, (c) segmentation marking of heart sounds.

Table 1

Performances of segmentation of the heart sound using different algorithms.

	Total heart sound	TP	FP	FN	Sensitivity (in %)	Positive predictive value (in %)	Accuracy (in %)
Proposed Algorithm	3669	3618	42	51	98.61	99.11	98.07
L-HSMM	3669	3623	63	46	98.75	97.82	96.82

the strength of S1 sound is prominent, whereas, the S2 sound is not clearly visible. Due to this, the residual signal contains strong peaks at the location of S1, whereas the S2 sounds contain small peaks which are not clearly visible, as shown in Fig. 12(b). Similar observation is also observed for MVP PCG signal contaminated with breathing noise shown in Fig. 13. Fig. 13(b) shows strong peaks in the residual signal at the locations of S1 sounds whereas the strength of peaks at S2 locations is not clearly visible. The residual output does not contain strong peaks at S2 sound location in both arrhythmia and MVP conditions. For both the cases, the small fluctuation in the residual output signal provides heart sound information for duration modelling. Therefore, the algorithm is able

to localize the heart sound effectively in both the cases shown in Fig. 12(c) and Fig. 13(c), respectively.

The effectiveness of the proposed algorithm is evaluated in lab environment. In this study, a PCG signal acquisition system is implemented [6]. The acquisition system includes an acoustic stethoscope, a microphone, a USB DAQ card, a breadboard and Labview software. The tube of stethoscope is attached to the microphone (make: Vernier, Model: MCA-BTA) with a rubber connector. The microphone is connected to the DAQ card (make: NI Model: NIUSB-6003). The condenser microphone is powered through the DAQ card. The audio PCG signal is digitized with a rate of 1000 samples per second and 16 bits resolution. The digitized PCG signal

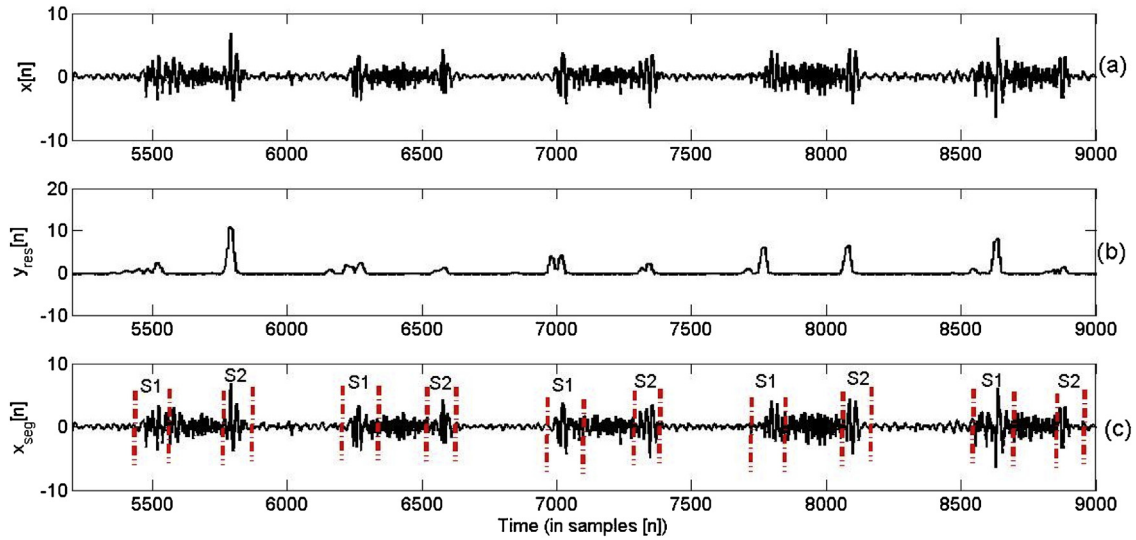


Fig. 10. Segmentation of heart sound taken from pathological condition aortic stenosis using proposed algorithm (a) PCG signal, (b) Residual output of ZFF (c) Segmentation of heart sound.

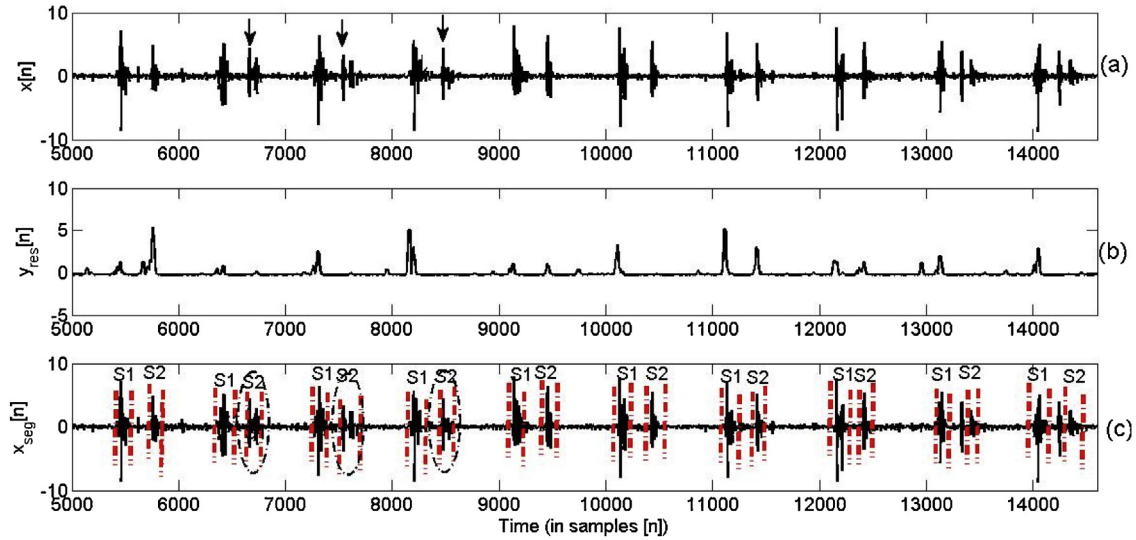


Fig. 11. Segmentation of heart sound taken from pathological condition MVP using proposed algorithm (a) PCG signal, (b) Residual output of ZFF (c) Segmentation of heart sound.

is recorded through LABview software and saved in Excel format. The PCG signal is further used in MATLAB software for heart sound segmentation.

Fig. 14 shows the segmentation of sounds S1 and S2 in the acquired PCG signal from a healthy person. In Fig. 14(b), residual signal shows peaks at heart sound locations. Therefore, heart sounds are effectively localized using the proposed algorithm.

The overall performances of the segmentation algorithms are now verified only for pathological PCG signals. The performance of segmentation is given in Table 2. The false negative and false positive of the proposed technique are 11 and 9, respectively whereas, the false negative and false positive of the LHSMM are 40 and 40, respectively. The algorithm is able to predict 97.26% heart sounds correctly for pathological PCG signals, whereas the LHSMM technique is able to predict 93.33% heart sounds correctly for pathological PCG signals. The proposed algorithm is also able to segment 96.52% heart sounds correctly, whereas LHSMM technique is able to segment 93.48% heart sounds correctly. The study inferred that the

proposed algorithm is able to localize the heart sound effectively in normal condition as well as in pathological condition.

3.1. Evaluation of heart sound algorithm under noisy conditions

3.1.1. White noise

A noise test is performed in order to verify the robustness of the proposed method against ambient noise. A recorded signal contains noise and the estimation of SNR level in a recorded signal is difficult. Therefore in present study, artificial noises with different SNR values of 30 dB, 20 dB and 10 dB are added to the PCG signals. The segmentation of heart sounds for SNR value of 10 dB is shown in Fig. 15. Fig. 15(b) shows that the proposed algorithm completely removes the effect of the noise as well as murmurs present in the signal. The algorithm gives clear peaks at the heart sound locations. Due to this, the segmentation algorithm is able to detect the heart sounds correctly in noisy conditions. For different SNR values of 30 dB, 20 dB and 10 dB, the detection performances of the proposed

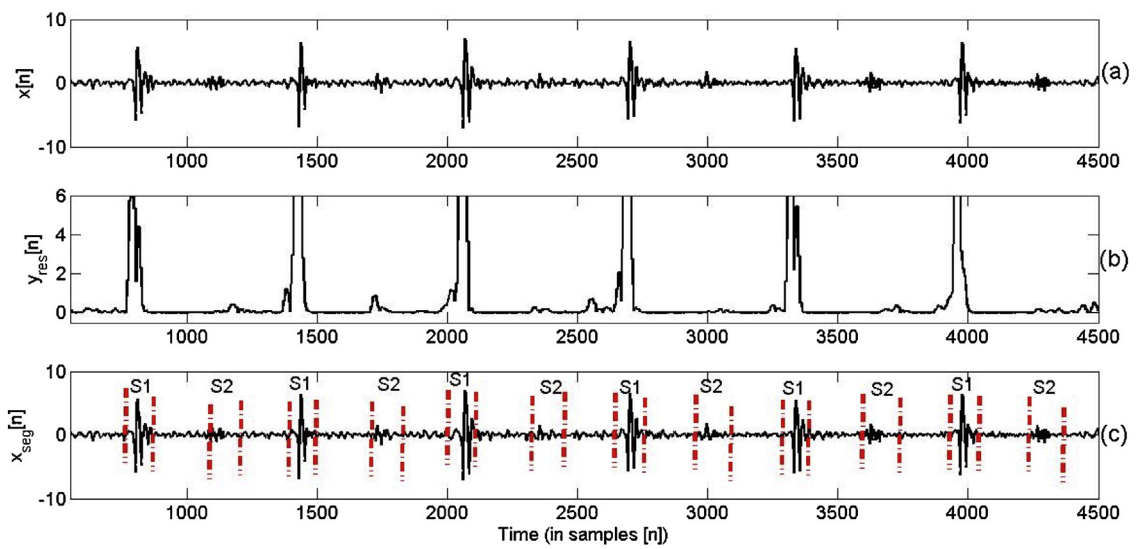


Fig. 12. Segmentation of heart sound taken from pathological condition arrhythmia using proposed algorithm (a) PCG signal, (b) Residual output of ZFF (c) Segmentation of heart sound.

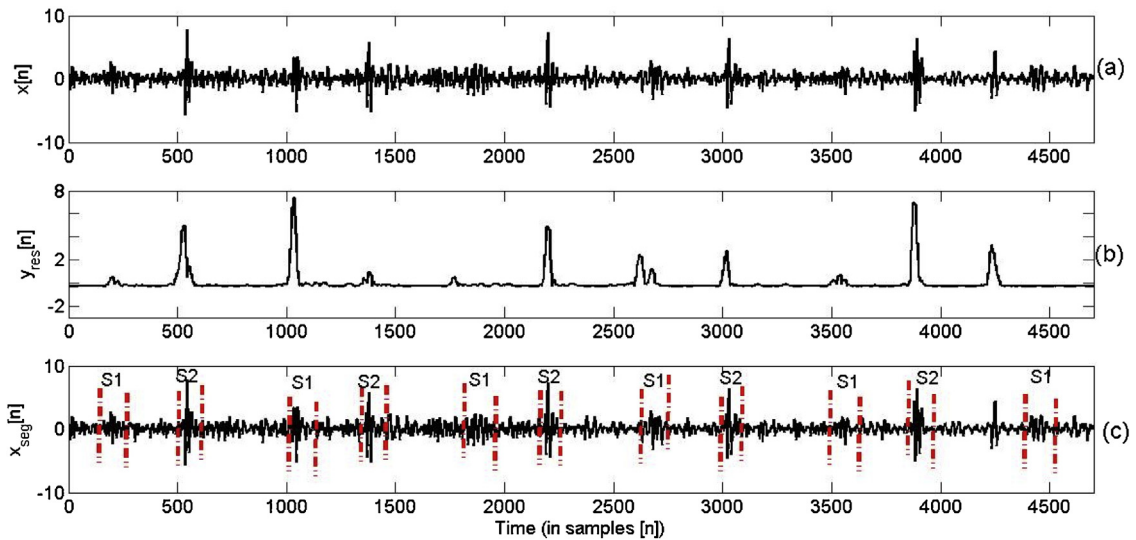


Fig. 13. Segmentation of heart sound taken from pathological condition Mitral Valve Prolapse contaminated by breathing noise using proposed algorithm (a) PCG signal, (b) Residual output of ZFF (c) Segmentation of heart sound.

Table 2

Performances of segmentation of the heart sound taken from pathological conditions using different algorithms.

	Total heart sound	TP	FP	FN	Sensitivity (in %)	Positive predictive value(in %)	Accuracy (in %)
Proposed Algorithm	534	523	9	11	96.52	97.26	93.93
L-HSMM	534	494	40	40	93.48	93.33	89.73

Table 3

Performance of segmentation algorithms for different dB SNR noise added to the PCG signal.

Proposed	Total heart sound	TP	FP	FN	Sensitivity (in %)	Positive predictive value(in %)	Accuracy (in %)
Original Signal	3669	3618	42	51	98.61	99.11	98.07
30 dB	3669	3624	44	54	98.52	99.23	98.29
20 dB	3669	3613	48	56	98.51	98.99	97.95
10 dB	3669	3612	47	57	98.47	98.81	97.47
L-HSMM	3669	3623	63	46	98.90	97.82	96.82
LHSMM	3669	3623	63	46	98.90	97.82	96.82
20 dB	3669	3623	64	47	98.83	97.81	96.80
10 dB	3669	3621	65	48	98.81	97.76	96.70

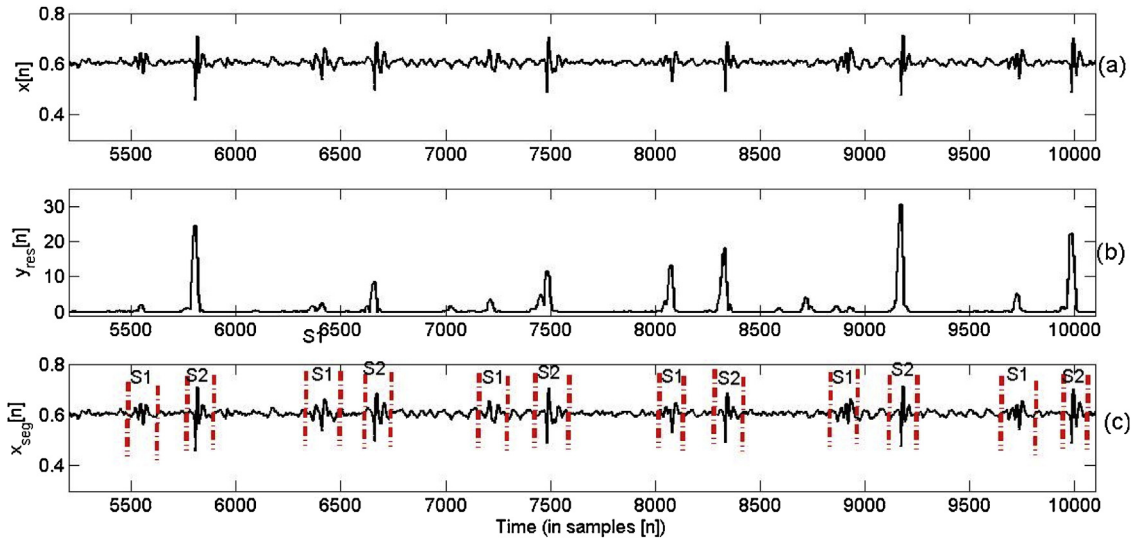


Fig. 14. Segmentation of heart sound taken acquired from lab environment. (a) PCG signal, (b) Residual output of ZFF (c) Segmentation of heart sound.

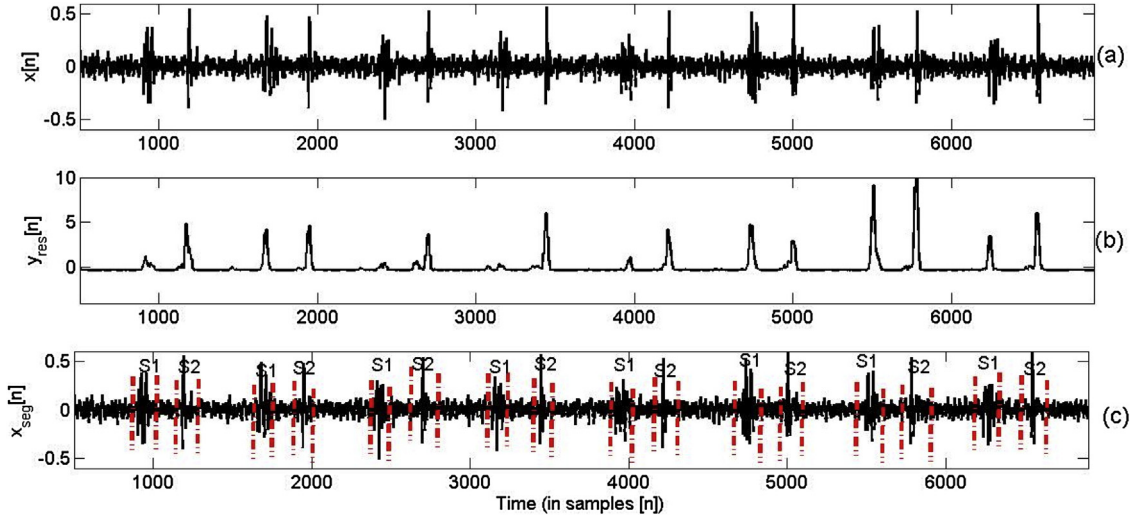


Fig. 15. Segmentation of heart sound of the PCG signal taken from MVP condition added with 10 dB white noise using proposed algorithm (a) PCG signal, (b) Residual output of ZFF (c) Segmentation of heart sound.

algorithm and LHSMM are tabulated in Table 3. From the result, it is observed that the proposed algorithm significantly improves the detection performance under low SNR condition as compared to that of LHSMM. For SNR value of 10 dB, the proposed algorithm achieves an average sensitivity of 98.47%, average positive predictive value of 98.81% and average overall accuracy of 97.47%, while, the LHSMM method has average sensitivity of 98.81%, average positive predictive value of 97.76% and average overall accuracy of 96.60%. From Table 3 it can be observed that the sensitivity of the proposed algorithm is less compared to that of LHSMM algorithm, while, the predictions and the overall accuracy of the proposed algorithm are higher than those of LHSMM algorithm.

3.1.2. Respiratory Noise

In Section 3.1.1, simulated noises of different SNR values are added to the PCG signal. Since, the simulated noise is uniform across time; the effect of time varying nature of noise is not taken into account. In the present section, a respiratory noise test is performed in order to evaluate the robustness of the proposed method

in time varying noise conditions. In this test, the PCG signal taken from MVP condition is added with two types of respiratory noises namely, bronchial and crackles. Lung sounds are taken from [33]. The lung sound signal is sampled at 44 kHz. First the lung sounds are resampled at 1000 Hz, then the amplitude of the respiratory noise is normalized in the range of [1,1]. Similarly, the amplitude of PCG signal is also normalized in the range of [1,1]. The resampled and normalized noises are added to the normalized PCG signal. The segmentation of heart sounds added with bronchial and crackles noises are shown in Fig. 16 and Fig. 17, respectively. From Fig. 16(a), it can be observed that unlike white noise, the bronchial noise is non-uniformly distributed over the signal. Some regions of the PCG signal are fully contaminated with noise. Fig. 16(b) shows that the effect of the noise is completely removed from the filtered output. The detection performances of heart sound segmentation using proposed algorithm and LSHMM are given in Table 4. The proposed algorithm produces a 63 FN and 42 FP for a total detection of 3669 heart sounds, while, LSHMM algorithm produces 47 FN and 64 FP for the same number of heart sounds. The proposed algo-

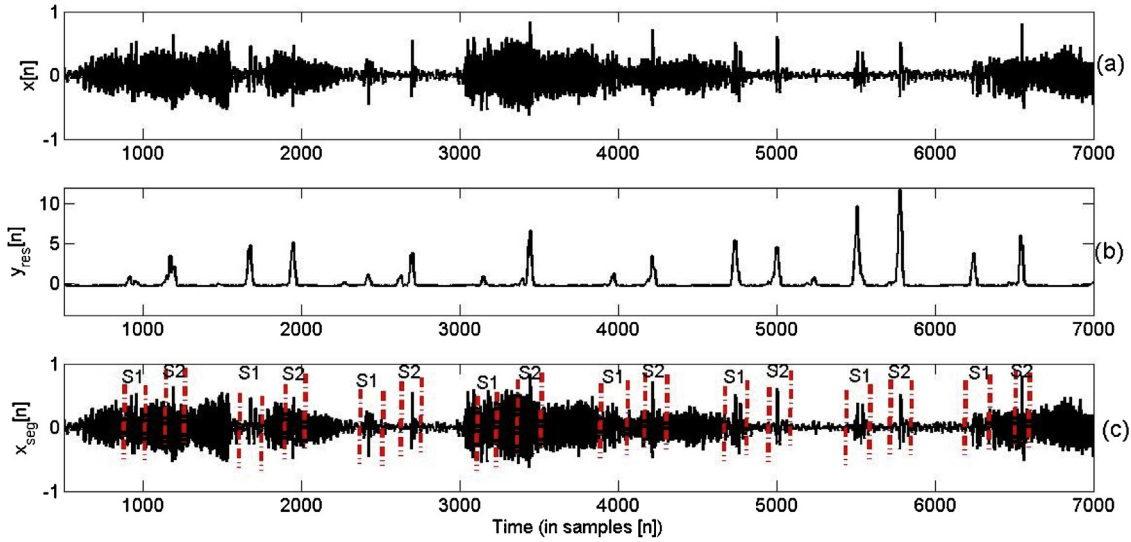


Fig. 16. Segmentation of heart sound of the PCG signal taken from MVP condition added with bronchial noise using proposed algorithm (a) PCG signal, (b) Residual output of ZFF (c) Segmentation of heart sound.

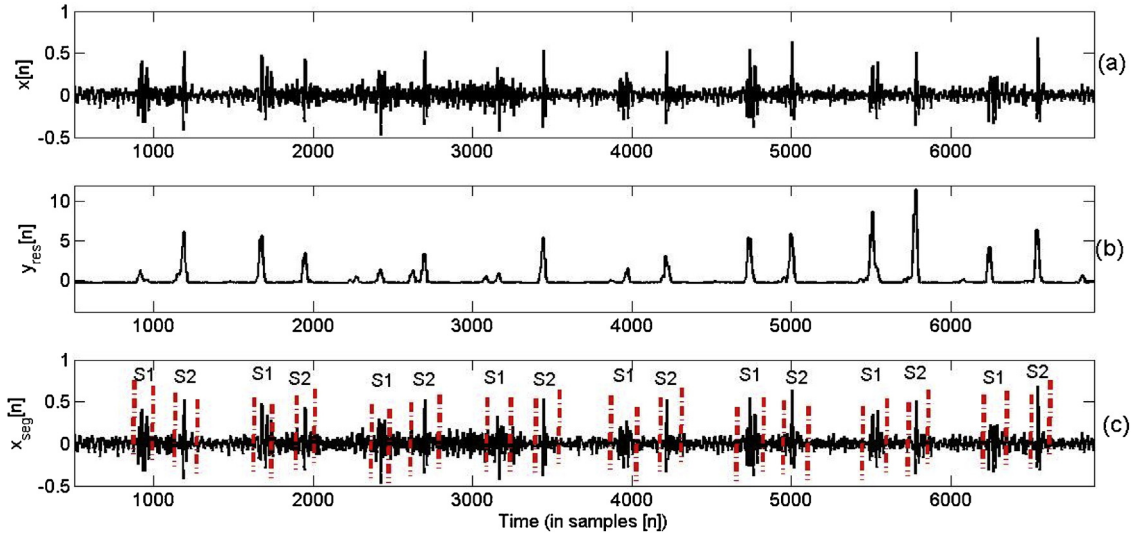


Fig. 17. Segmentation of heart sound of the PCG signal taken from MVP condition added with crackles noise using proposed algorithm (a) PCG signal, (b) Residual output of ZFF (c) Segmentation of heart sound.

Table 4

Performance of segmentation algorithms for different respiratory noises added to the PCG signal.

Proposed	Total heart sound	TP	FP	FN	Sensitivity (in %)	Positive predictive value (in %)	Accuracy (in %)
Bronchial	3669	3546	42	63	98.31	98.87	97.22
Crackles	3669	3595	56	74	97.98	98.47	96.51
L-HSMM							
Bronchial	3669	3622	64	47	98.72	98.26	97.03
Crackles	3669	3620	64	49	98.61	98.21	96.92

rithm achieves an average sensitivity of 98.31%, average positive predictive value of 98.87% and average overall accuracy of 97.22%, while, the LHSMM method has average sensitivity of 98.72%, average positive predictive value of 98.26% and average overall accuracy of 97.03%. Hence, the overall accuracy and predictive value are higher in proposed algorithm compared to that of LHSMM. Similar results are obtained for the PCG signal added with crackle noise. Crackles are short discontinuous explosive sounds. Segmentation of the heart sound of the PCG signal with MVP condition and crackle noise is shown in Fig. 17. Fig. 17(b) shows that the effect of discontinuous explosive sound is also removed from the filtered output.

Hence, the algorithm is able to localize better the heart sound. From Table 4, it can be observed that the proposed algorithm produces a 74 FN and 56 FP for a total detection of 3669 heart sounds, while, LSHMM algorithm produces 49 FN and 64 FP for the same number of heart sounds. The proposed algorithm achieves an average sensitivity of 97.98%, average positive predictive value of 98.47% and average overall accuracy of 96.51%, while, the LHSMM method has average sensitivity of 98.61%, average positive predictive value of 98.21% and average overall accuracy of 96.92%. Hence, the proposed algorithm has higher accuracy and predictive value compared to the LHSMM.

From the above experiments, it can be observed that the proposed algorithm is efficient in heart sound segmentation in both clean and noisy conditions including different pathological conditions. The amplitude dependent threshold techniques [8,9,17], sometimes, miss the genuine peaks with less energy and accept the noisy peaks with more energy. The proposed algorithm detects the abrupt changes at the heart sound locations. Therefore, the algorithm is able to discriminate between heart sounds and murmur characteristics occurring due to pathological conditions. Also, this technique does not require any search back operation to detect genuine peaks with less energy. Hence, the proposed method can be suitable for cardiac monitoring applications.

4. Conclusion

A novel approach for heart sound segmentation is proposed. The abrupt change at the occurrence of the heart sound is considered as a cue factor for heart sound segmentation. The kurtosis of the enveloped signal is taken to increase the impulsiveness at the heart sound location. The impulsive characteristics at heart sound locations are obtained by passing kurtosis signal through ZFF. The impulsive characteristic of the signal is used for heart sound segmentation. The effectiveness of the proposed algorithm is verified with an experimental dataset taken from real clinical environment, including normal heart sound and pathological heart sounds. Result shows that the proposed algorithm performs better compared to state of the art technique LHSMM. The positive predictive value and overall accuracy of the proposed method are higher than those of LHSMM. The robustness of the proposed algorithm is also verified by adding white Gaussian noise and time varying respiratory noises to the PCG signal.

Acknowledgment

This work is supported by research grant from Science & Engineering Research Board India, through project File No. PDF/2017/002343.

Declaration of Competing Interest

The authors declare that they have no known competing financial interests or personal relationships that could have appeared to influence the work reported in this paper

References

- [1] WHO, World Statistics on Cardiovascular Disease, 2015 www.who.int/mediacentre/factsheets/fs317/en/.
- [2] V.N. Varghees, K.I. Ramachandran, A novel heart sound activity detection framework for automated heart sound analysis, *Biomed. Signal Process. Control* 13 (2014) 174–188, <http://dx.doi.org/10.1016/j.bspc.2014.05.002>.
- [3] R.J. Lehner, R.M. Rangayyan, A three-channel microcomputer system for segmentation and characterization of the phonocardiogram, *IEEE Trans. Biomed. Eng.* 34 (6) (1987) 485–489, <http://dx.doi.org/10.1109/TBME.1987.326060>.
- [4] X. Zhang, L.G. Durand, L. Senhadji, H.C. Lee, J.L. Coatrieux, Analysis-synthesis of the phonocardiogram based on the matching pursuit method, *IEEE Trans. Biomed. Eng.* 45 (8) (1998) 962–971, <http://dx.doi.org/10.1109/10.704865>.
- [5] C.D. Papadaniil, L.J. Hadjileontiadis, Efficient heart sound segmentation and extraction using ensemble empirical mode decomposition and kurtosis features, *IEEE EMBS. Int. Conf. Biomed. Health Inform.* 18 (4) (2014) 1138–1152, <http://dx.doi.org/10.1109/JBHI.2013.2294399>.
- [6] V.N. Varghees, K.I. Ramachandran, Effective heart sound segmentation and murmur classification using empirical wavelet transform and instantaneous phase for electronic stethoscope, *IEEE Sensor* 17 (12) (2017) 3861–3872, <http://dx.doi.org/10.1109/JSEN.2017.2694970>.
- [7] T. Oskiper, R. Watrous, Detection of the first heart sound using a time-delay neural network, *First Heart Sound Using a Time-delay Neural Network*, in: *Computers in Cardiology*, Memphis, tn, USA, Sept., 2002, pp. 537–540, <http://dx.doi.org/10.1109/CIC.2002.1166828>.
- [8] T. Olmez, Z. Dokur, Classification of heart sounds using an artificial neural network, *Pattern Recogn. Lett.* 24 (1–3) (2003) 617–629, [http://dx.doi.org/10.1016/S0167-8655\(02\)00281-7](http://dx.doi.org/10.1016/S0167-8655(02)00281-7).
- [9] H. Liang, S. Lukkarinen, I. Hartimo, A heart sound segmentation algorithm using wavelet decomposition and reconstruction, Chicago, IL, USA, in: *Proceedings of the 19th Annual International Conference of the IEEE Engineering in Medicine and Biology Society: Magnificent Milestones and Emerging Opportunities in Medical Engineering* (Cat. No.97CH36136), vol. 4, 1997, pp. 1630–1633, <http://dx.doi.org/10.1109/EMBS.1997.757028>.
- [10] P. Wang, Y. Kim, L.H. Ling, C.B. Soh, First heart sound detection for phonocardiogram segmentation, in: *IEEE Engineering in Medicine and Biology 27th Annual Conference*, Shanghai, 2005, pp. 5519–5522, <http://dx.doi.org/10.1109/EMBS.2005.1615733>.
- [11] S. Jabbari, H. Ghassemian, A time-frequency approach for discrimination of heart murmurs, *J. Signal Inform. Proc.* 2 (August (3)) (2011) 232–237, <http://dx.doi.org/10.4236/jsip.2011.23032>.
- [12] A.P. Kamson, L.N. Sharma, S. Dandapat, Detection of heart sound using logistic function amplitude moderator and Teager-Kaiser energy operator, in: *International Conference on Signal Processing and Communications (SPCOM)*, Bangalore, India, 2018, pp. 422–426, <http://dx.doi.org/10.1109/SPCOM.2018.8724410>.
- [13] K. Courtemanche, V. Millette, N. Baddour, Heart sound segmentation based on Mel-scaled wavelet transform, *CMBES* 31 (1) (2017).
- [14] X. Zhang, L. Durand, L. Senhadji, H.C. Lee, J.L. Coatrieux, Analysis-synthesis of the phonocardiogram based on the matching pursuit method, *IEEE Trans. Biomed. Eng.* 45 (8) (1998) 962–971, <http://dx.doi.org/10.1109/10.704865>.
- [15] Z. Zhao, Z. Zhao, Y. Chen, Time-frequency analysis of heart sound based on HHT [Hilbert-Huang transform], in: *Proceedings. 2005 International Conference on Communications, Circuits and Systems*, Hong Kong, China, 2005, pp. 926–929, <http://dx.doi.org/10.1109/ICCCAS.2005.1495260>.
- [16] A. Moukadem, A. Dieterlen, N. Hueber, Christian Brandt, A robust heart sounds segmentation module based on S-transform, *Biomed. Signal Process. Control* 8 (3) (2013) 273–281, <http://dx.doi.org/10.1016/j.bspc.2012.11.008>.
- [17] H. Liang, S. Lukkarinen, I. Hartimo, Heart sound segmentation algorithm based on heart sound envelopegram, in: *Computers in Cardiology 1997*, Lund, Sweden, Sept., 1997, pp. 105–108, <http://dx.doi.org/10.1109/CIC.1997.647841>.
- [18] Z. Yan, Z. Jiang, A. Miyamoto, Y. Mie, The moment segmentation analysis of heart sound pattern, *Comput. Methods Progr. Biomed.* 98 (2) (2010) 140–150, <http://dx.doi.org/10.1016/j.cmpb.2009.09.008>.
- [19] A. Sepehri, A.G.T. Dutoit, A. Kocharian, A. Kiani, A novel method for pediatric heart sound segmentation without using the ECG, *Comput. Methods Progr. Biomed.* 99 (1) (2010) 43–48, <http://dx.doi.org/10.1016/j.cmpb.2009.10.006>.
- [20] M. Fanfulla, M. Malcangi, M. Riva, D.D. Giustina, F. Belloni, Cardiac sounds segmentation algorithm for arrhythmias detection by fuzzy logic, *Int. J. Circuits Syst. Signal Process.* 5 (2011) 192–200.
- [21] H. Tang, T. Li, T. Qiu, Y. Park, Segmentation of heart sounds based on dynamic clustering, *Biomed. Signal Process. Control* 7 (5) (2012) 509–516, <http://dx.doi.org/10.1016/j.bspc.2011.09.002>.
- [22] D. Gill, N. Gavrielli, N. Intrator, Detection and identification of heart sounds using homomorphic envelopegram and self-organizing probabilistic model, *Computers in Cardiology (2005)* 957–960, <http://dx.doi.org/10.1109/CIC.2005.1588267>, Lyon, Sept.
- [23] D.B. Springer, L. Tarassenko, G.D. Clifford, Logistic regression-HSMM-based heart sound segmentation, *IEEE Trans. Biomed. Eng.* 63 (4) (2016) 822–832, <http://dx.doi.org/10.1109/TBME.2015.2475278>.
- [24] Alex Paul Kamson, L.N. Sharma, S. Dandapat, Multi-centroid diastolic duration distribution based HSMM for heart sound segmentation, *Biomed. Signal Process. Control* 48 (2019) 265–272, <http://dx.doi.org/10.1016/j.bspc.2018.10.018>.
- [25] K.S.R. Murty, B. Yegnanarayana, Epoch extraction from speech signals, *IEEE Trans. Audio, Speech, Lang. Proc.* 16 (8) (2008) 1602–1613, <http://dx.doi.org/10.1109/TASL.2008.2004526>.
- [26] P. Borghesani, P. Pennacchi, S. Chatterton, The relationship between kurtosis- and envelope-based indexes for the diagnostic of rolling element bearings, *Mech. Syst. Signal Process.* 43 (1–2) (2014) 25–43, <http://dx.doi.org/10.1016/j.ymssp.2013.10.007>.
- [27] A.C. Guyton, J.E. Hall, *Textbook of Medical Physiology*, 11th edition, Elsevier Saunders, Amsterdam, 2006.
- [28] G. Strang, *Linear Algebra and Its Applications*, 4th edn., Cengage Learning, Boston, 2006.
- [29] K. Kumar, S. Shukla, S.K. Singh, A combined approach for weak fault signature extraction of rolling element bearing using Hilbert envelop and zero frequency resonator, *J. Sound Vib.* 419 (2018) 436–451, <http://dx.doi.org/10.1016/j.jsv.2018.01.022>.
- [30] B. Yegnanarayana, K.S.R. Murty, Event-based instantaneous fundamental frequency estimation from speech signals, *IEEE Trans. Audio Speech Lang. Proc.* 17 (4) (2009) 614–624, <http://dx.doi.org/10.1109/TASL.2008.2012194>.
- [31] C. Liu, D. Springer, Q. Li, B. Moody, R.A. Juan, F.J. Chorro, F. Castells, J.M. Roig, I. Silva, A.E. Johnson, et al., An open access database for the evaluation of heart sound algorithms, *Physiol. Meas.* 37 (12) (2016) 2181–2213, <http://dx.doi.org/10.1088/0967-3334/37/12/2181>.
- [32] (Apr. 10, 2017). PhysioNet/CinC Challenge 2016. [Online]. Available: <https://www.physionet.org/challenge/2016/>.
- [33] Thinklabs Stethoscopes Lung Sound Library, 2018 (Oct. 20, 2018) [Online]. Available https://www.youtube.com/channel/UCzEbKulze4Al1523_AWiK4w.